Cronfa - Swansea University Open Access Repository

_____

This is an author produced version of a paper published in:
ACS Applied Energy Materials

_____

Cronfa URL for this paper:

_____

Paper:

_____

Monte Carlo Simulations of Electron Transport Characteristics of Ternary Carbide Al$_4$SiC$_4$

Simon Forster,*,[†,‡] Didier Chaussende,[‡] and Karol Kalna[†]

[†]Nanoelectronic Devices Computational (NanoDeCo) Group, College of Engineering, Swansea University, Swansea SA1 8EN, Wales, United Kingdom

[‡]Université Grenoble Alpes, CNRS, Grenoble INP, SIMAP, 38000 Grenoble, France

ABSTRACT: Electron transport characteristics of a novel wide band gap ternary carbide, Al$_4$SiC$_4$, to be used for efficient power and optoelectronic applications, are predicted using ensemble Monte Carlo (MC) simulations. The MC simulations use a mixture of material parameters obtained from density functional theory (DFT) calculations and experiment, with a preference for the experimental data if they are known. The DFT calculations predict a band gap of 2.48 eV, while the experimental measurements give a band gap between 2.78 and 2.8 eV. We have found that the electron effective mass in the two lowest valleys (M and K) is highly anisotropic; in the K valley, $m_t^* = 0.5678\ m_e$ and $m_l^* = 0.6952\ m_e$, and for the M valley, $m_t^* = 0.9360\ m_e$ and $m_l^* = 1.0569\ m_e$. We simulate electron drift velocity and electron mobility as a function of applied electric field as well as electron mobility as a function of doping concentration in Al$_4$SiC$_4$. We predict a peak electron drift velocity of 1.35×10^7 cm s^{-1} at an electric field of 1400 kV cm^{-1} and a maximum electron mobility of 82.9 cm^2 V^{-1} s^{-1}. We have seen diffusion constants of 2.14 cm^2 s^{-1} at a low electric field and 0.25 cm^2 s^{-1} at a high electric field. Finally, we show that Al$_4$SiC$_4$ has a critical field of 1831 kV cm^{-1}.

KEYWORDS: ensemble Monte Carlo, ternary carbide, Al$_4$SiC$_4$, effective mass, electron transport, breakdown
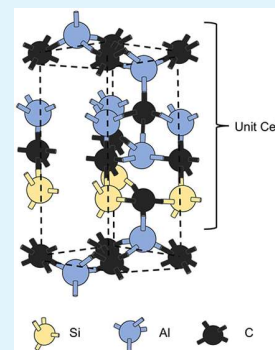
1. INTRODUCTION

Al$_4$SiC$_4$, a wide band gap ternary carbide semiconductor material, has attracted a great deal of interest from the electronics industry over the past decade because of its emerging semiconductor properties, a departure from its previous classification as a ceramic material.[1,2] Although the material was first computed as having a band gap of only 1.05 eV,[3] the band gap has been re-evaluated to be 2.48 eV[4−6] in recent years. This has led to Al$_4$SiC$_4$ being classified as a wide band gap semiconductor, with a band gap very close to that of, for instance, 3C-SiC and thus potentially addressing similar fields of applications. Other properties that have been documented for this material include superior oxidation resistance,[7,8] superior wear resistance, low weight, high strength, and high thermal conductivity.[9] These material properties mean that Al$_4$SiC$_4$ could become a very useful and versatile material in applications for the optoelectronics and power electronics industry.

Al$_4$SiC$_4$ is currently being studied by several research groups[5,7,8,10−14] that are looking to find a practical way to fabricate the material in crystalline form.[15] Theoretical investigations, primarily density functional theory (DFT) calculations of a band structure, have been carried out for Al$_4$SiC$_4$[2−4,16,17] to determine its material properties and assist in experimental characterization. Other investigations have looked at the optical, ac electrical, thermal, and some mechanical properties of Al$_4$SiC$_4$,[16,18] including a combined study of the structural and mechanical properties of Al$_4$SiC$_4$.[1] Dunia et al.[18] examined the electrical properties of Al-SiC

composites with measured values for the ac electrical conductivity and dielectric constant over a frequency range of 200 Hz to 6 GHz. They suggest two frequency-dependent mechanisms for conduction in Al-SiC composites along with dielectric constants following a semi-steady state behavior over the frequency range. Liao et al.[1] investigated the bonding characteristics, elastic stiffness, and ideal strength showing that the mechanical properties are closely related to the crystal structure of Al$_4$SiC$_4$ giving a bulk modulus of 179 GPa, a shear modulus of 140 GPa, and lattice parameters of $a = 3.222$ Å and $c = 21.352$ Å. Similar mechanical properties were described by Sun et al.[16] and Liao et al.[1] with additional investigation into the thermal properties of Al$_4$SiC$_4$. The heat capacity was shown over a temperature range of 200−2000 K, where the heat capacity rapidly increased at low temperatures while the rate of change slowed at high temperatures (>500 K).

In this work, we have employed an in-house bulk ensemble Monte Carlo (MC) simulation code[19,20] to determine the electron transport properties of Al$_4$SiC$_4$. The MC simulations use a combination of known material properties from reported experimental data and theoretical calculations using DFT. Detailed predictions of the electronic transport properties of Al$_4$SiC$_4$ are completely missing from the literature.

Al$_4$SiC$_4$ has a hexagonal lattice[3−6,14,21,22] comprising multiple valleys, Γ, A, L, H, M, and K, as shown in Figure 1 and
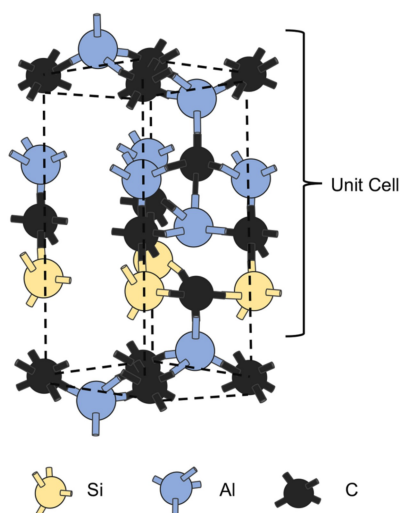
Figure 1. Crystal structures of Al_4SiC_4. The blue, yellow, and black spheres represent Al, Si, and C atoms, respectively.
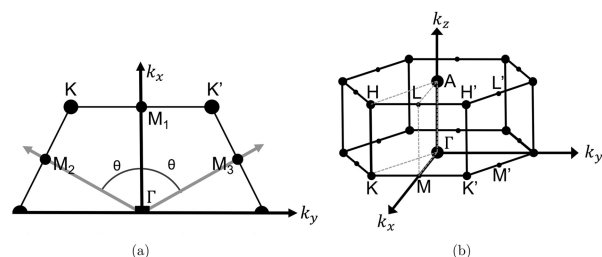
panels a and b of Figure 2. We will demonstrate that only the two lowest valleys, the M and K valleys, are of interest for

Figure 2. (a) Hexagonal (0001) plane showing the location of the M valleys within the Al_4SiC_4 hexagonal structure, where $\theta = \pm 60°$. (b) Hexagonal structure showing the location of principal valleys.

electron transport as the occupation of all other upper valleys is negligible. The MC simulations predict that Al_4SiC_4 will have a maximum electron drift velocity of 1.35×10^7 cm s^{-1} at an electric field of 1400 kV cm^{-1} and a maximum electron mobility of 82.9 cm^2 V^{-1} s^{-1}. We also show what is the dependence of the electron mobility on the ionized impurity concentration in Al_4SiC_4. We predict a steady diffusion constant of approximately 0.25 cm^2 s^{-1} at a high electric field of 1400 kV cm^{-1}. Finally, we show that the critical field for Al_4SiC_4 is 1831 kV cm^{-1}.

The paper is organized as follows. Section 2 gives details about material parameters and the physical model used, a bulk ensemble MC simulation. Section 3 outlines a rotational valley transformation that has been introduced in this work for the particular band structure of Al_4SiC_4. Section 4 presents the results and discusses them. Finally, section 5 draws a conclusion.

2. MONTE CARLO SIMULATIONS

We have adapted an ensemble bulk MC simulation code to investigate the electron transport in bulk Al_4SiC_4. The simulation considers bulk properties of Al_4SiC_4 when electron transport can be considered to be free in three-dimensional **k** space. We have employed a two-valley model for the conduction band of Al_4SiC_4 based on the band structure

obtained by Pedesseau et al.[4] as seen in Figure 3. The two arrows in this figure indicate the two valleys that we are
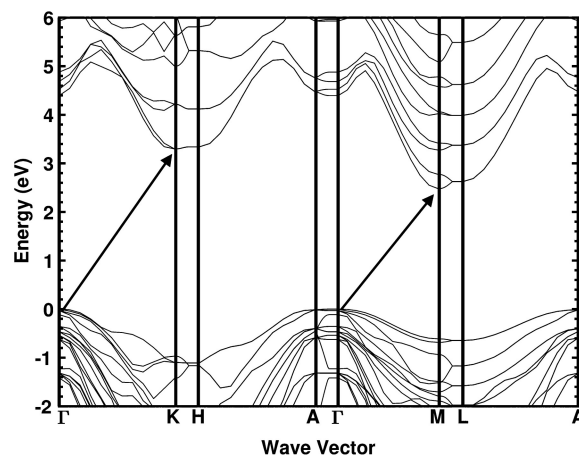
Figure 3. Rescaled Al_4SiC_4 band structure obtained from DFT calculations from ref 4. The two black arrows indicate the two valleys that we considered in the MC simulations.

considering in a simulation model. The first valley, the M valley, is situated 2.78 eV above the valence band maximum of the Γ valley and is an indirect band gap. The second valley, the K valley, is situated 0.52 eV above the M valley (see Figure 4) and has also an indirect band gap.
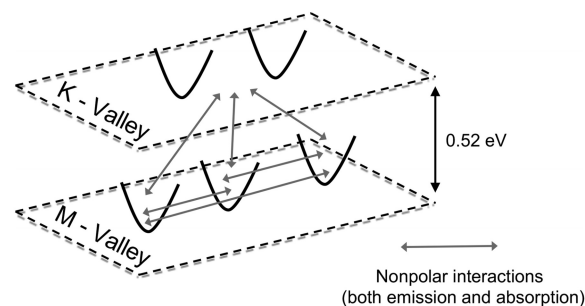
Figure 4. Schematic of conduction band minimum valleys in Al_4SiC_4 showing the number of equivalent bands in each valley and the separation between the two considered valleys.

However, to date this band gap has been estimated to be anywhere between 1.05 and 2.5 eV according to various authors who have published their work on Al_4SiC_4. A summary of these works is shown in Table 1, indicating the value of the band gap. We have chosen to use the value of 2.78 eV for the

Table 1. Comparison of Published Energy Band Gaps for Al_4SiC_4 Indicating a Method and a Source

published band gap (eV)	method
1.05	computational (DFT)[3]
1.12	computational (DFT)[16]
1.81	computational (DFT)[17]
2–2.5	experiment (UV–vis–NIR)[5]
2.48	computational (DFT), experimental (ellipsometry)[4]
2.4–2.5	experiment (UV–vis–NIR and ellipsometry)[6]

band gap as this has been obtained in our experimental work.[23] A majority of the DFT simulations to date have shown a lower value for the band gap of <2.0 eV, which is an underestimation of the band gap often observed in DFT calculations of wide band gap materials.[24]

Figure 4 includes the number of equivalent bands that have been identified for the two valleys of interest for MC simulations. The number of equivalent valleys in each of the two valleys is based on the hexagonal lattice that Al_4SiC_4 is known to have.[3−6,14,21,22] Figure 2a shows that the K valley is present in six locations, each of which contributes one-third to the first Brillouin zone leading to a total of two equivalent bands. The M valley is present in six locations similar to the K valleys. However, because of their positions between the K valleys, each of these six M valleys contributes one-half to the first Brillouin zone, leading to a total of three equivalent bands. The band structure model of Al_4SiC_4 is an analytical nonparabolic anisotropic band structure.[25] We have considered the following electron scattering mechanisms in the MC simulations that will play a decisive role in electron transport (see Table 2): electron interactions with acoustic phonons,

Table 2. Electron−Phonon Scattering Transitions Considered in the MC Model

valley	scattering between	polar or nonpolar	inter- or intravalley
M_1	$M_1 \rightarrow M_1$	polar	intra
	$M_1 \rightarrow M_1$	polar	intra
	$M_1 \rightarrow M_2$	nonpolar	inter
	$M_1 \rightarrow M_3$	nonpolar	inter
	$M_1 \rightarrow K$	nonpolar	inter
M_2	$M_2 \rightarrow M_2$	polar	intra
	$M_2 \rightarrow M_2$	polar	intra
	$M_2 \rightarrow M_1$	nonpolar	inter
	$M_2 \rightarrow M_3$	nonpolar	inter
	$M_2 \rightarrow K$	nonpolar	inter
M_3	$M_3 \rightarrow M_3$	polar	intra
	$M_3 \rightarrow M_3$	polar	intra
	$M_3 \rightarrow M_1$	nonpolar	inter
	$M_3 \rightarrow M_2$	nonpolar	inter
	$M_3 \rightarrow K$	nonpolar	inter
K	$K \rightarrow M_1$	nonpolar	inter
	$K \rightarrow M_2$	nonpolar	inter
	$K \rightarrow M_3$	nonpolar	inter

with polar and nonpolar optical phonons, and with ionized impurities when simulating electron transport properties in an n-type doped Al_4SiC_4.

The MC simulations assume a crystal temperature at 300 K and the orientation of the applied electric field along the ⟨0001⟩ crystallographic direction of the hexagonal lattice structure.[3−6,14,21,22] The material parameters, including parameters for electron−phonon interactions, are listed in Table 3. In the case of acoustic deformation potential, we have opted for the value reported for 4H-SiC[26] as the closest semiconductor material to Al_4SiC_4 with a well-known electron−phonon deformation potential because an acoustic deformation potential is currently unknown in Al_4SiC_4.

A critical electric field of Al_4SiC_4 is calculated using eq 1 as[27]

$$\varepsilon_c = a(E_G)^n \tag{1}$$

where $a = 2.3818 \times 10^5$ and $n = 1.995$ for an indirect band gap semiconductor and E_G is the band gap of the semiconductor.

Table 3. Material Parameters of Al_4SiC_4

mass density (g/cm³)	3.03^a
lattice constant (Å)	3.28^a
piezoelectric constant (C/m²)	0.47^a
longitudinal acoustic velocity (m/s)	10577^a
transverse acoustic velocity (m/s)	6431^a
polar optical phonon energyies (meV)	$67.32,^b\ 107.24^b$
nonpolar optical phonon energy (meV)	85.55^b
acoustic deformation potential (eV)	$11.4q^c$
indirect band gap (eV)	$E_G^{(M)} = 2.78\ M$ valley
	$E_G^{(K)} = 3.30^a\ K$ valley
electron effective mass	$m_l^{*(M)} = 0.5678\ m_e^d$
	$m_t^{*(M)} = 0.6952\ m_e^d$
	$m_l^{*(K)} = 1.0569\ m_e^d$
	$m_t^{*(K)} = 0.9360\ m_e^d$

^{a}From ref 4. ^{b}From ref 5. ^{c}Average taken from ref 26. ^{d}Extracted value from DFT calculations.[4]

Assuming a band gap of 2.78 eV, we obtain a critical electric field of 1831 kV cm⁻¹ for Al_4SiC_4. This critical electric field is well below the maximum electric field of 1400 kV cm⁻¹ we have simulated.

The optical phonon energies that have been used in these simulations have been extracted from IR/Raman spectroscopy from the works of Zevgitis et al.[7] Here, we have taken the three highest peaks in the $Z(XX)Z$ polarization configuration, where one would expect to see only A_1 and E_2 modes. The first peak we have taken is at a wavenumber of 690 cm⁻¹, which relates to an energy of 85.55 meV, and is an E_2, nonpolar mode, longitudinal optical phonon. The second peak is at a wavenumber of 543 cm⁻¹, which relates to an energy of 67.32 meV, and is an A_1, polar mode, transverse optical phonon. Finally, the third peak is at a wavenumber of 865 cm⁻¹, which relates to an energy of 107.25 meV, and is an A_1, polar mode, longitudinal optical phonon.

At the moment, a specific relationship between vibrational states and electrons is not clear with respect to which vibrational states directly contribute to or hinder the electron mobility. The electron effective masses in Table 3 have been extracted from DFT calculations by Pedesseau et al.[4] Here, we have assumed that the minima of the conduction band have a parabolic energy dispersion. The relative effective mass, m^*, can be then extracted from the following relation:

$$\frac{1}{m^*} = \frac{1}{\hbar^2}\frac{\partial^2 E(\vec{k})}{\partial k^2} \tag{2}$$
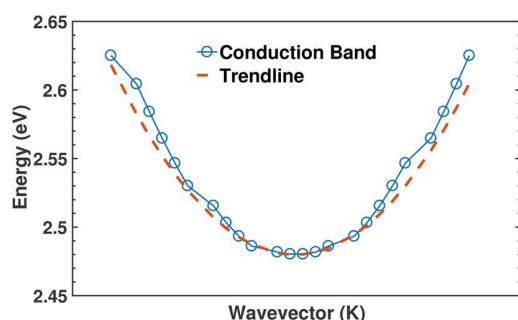
The dispersion relation is a quadratic polynomial, as illustrated in Figure 5, in the form $y = b + c_1 x + c_2 x^2$. The second-order derivative, $2c_2$, is related to the energy dispersion relation in eq 2 as

$$2c_2 = \frac{\partial^2 E(\vec{k})}{\partial k^2} \tag{3}$$

Equation 2 is solved for the M and K valleys in both the longitudinal and transverse directions giving the values of relative effective masses shown in Table 3.

3. WAVE-VECTOR TRANSFORMATIONS FOR THE M VALLEY

The location of the principal electron valley, M, in the Brillouin zone requires that components of electron wave-vectors in the

Figure 5. Dispersion relation in a conduction band fitted with a polynomial trend line.

Figure 6. Electron drift velocity (blue squares) as a function of applied electric field in bulk Al_4SiC_4 on the left axis. Electron mobility (red circles) as a function of applied electric field in bulk Al_4SiC_4 on the right axis.

band structure anisotropic analytical model of MC simulations be transformed accordingly. Therefore, we have enhanced our MC code with the wave-vector transformations that include a combination of Herring–Vogt transformation[28] and a rotational transformation of valleys.

The rotational transformation applied to the M valleys looks at transforming from elliptical space **k**-vector components, k_x, k_y, and k_z, to spherical vector components, k_x^*, k_y^*, and k_z^*, while considering the angular distance that the M_2 and M_3 valleys have in relation to the M_1 valley, our reference valley, located along the k_x direction as illustrated in Figure 2a. The angular distance that the M_2 and M_3 valleys have in relation to the M_1 valley can be defined along the k_x and k_y axes, as these valleys are rotated about the k_z axis (the k_z axis does not need to be transformed). The **k**-vector transformations for each of the components are defined as

$$k_x^* = k_x \cos(\theta) - k_y \sin(\theta) \tag{4}$$

$$k_y^* = k_y \cos(\theta) + k_x \sin(\theta) \tag{5}$$

$$k_z^* = k_z \tag{6}$$

In eqs 4–9, θ represents the angular distance the M_2 or M_3 valley rotates from the M_1 valley. The inverse transformations are given by
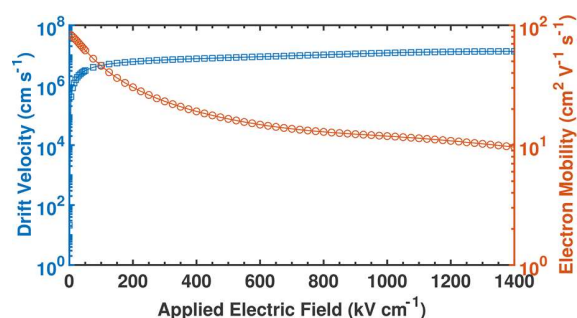
$$k_x = k_x^* \cos(\theta) + k_y^* \sin(\theta) \tag{7}$$

$$k_y = k_y^* \cos(\theta) - k_x^* \sin(\theta) \tag{8}$$

$$k_z = k_z^* \tag{9}$$

Finally, we assume an isotropic valley approximation for the K valleys due to their low electron occupation.

4. ELECTRON TRANSPORT PROPERTIES OF AL₄SIC₄

Figure 6 illustrates the electron drift velocity as a function of the applied electric field. The figure shows the applied electric field in a range from 0.01 to 1400 kV cm^{-1}. The electron velocity increases with an increasing electric field quickly at a relatively low electric field and starts to saturate at an electric field of ~200 kV cm^{-1}. At an applied electric field of 1400 kV cm^{-1}, the maximum drift velocity is approximately 1.35×10^7 cm s^{-1}, at which point the electron velocity is very well saturated. This saturation is caused by a strong emission of two polar optical phonons at energies of 67 and 107 meV (see Table 3). The average kinetic energy as a function of applied electric field is plotted in Figure 7. The kinetic energy increases
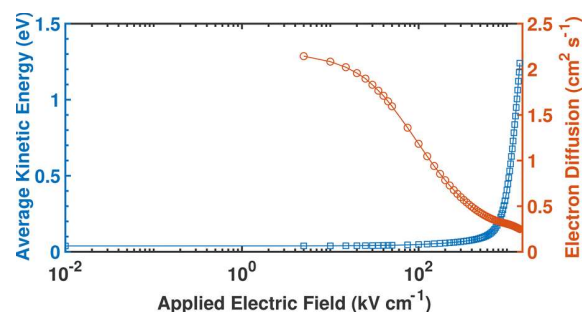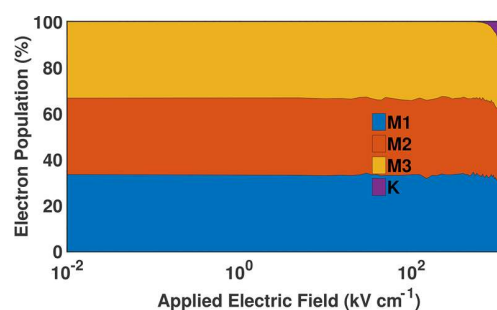

Figure 7. Average electron kinetic energy (blue squares) as a function of the applied electric field in bulk Al_4SiC_4 at the left. Electron diffusion (red circles) as a function of the applied electric field in bulk Al_4SiC_4 at the right.

approximately linearly as the electric field increases considering that the electric field is plotted on a logarithmic scale. We have monitored the electron kinetic energy that is larger than the band gap of Al_4SiC_4 in the simulations. At the largest electric field of 1400 kV cm^{-1} occurring in the simulations in Figures 7 and 8, the number of electrons over this energy amounts to

Figure 8. Stacked plot of the calculated valley occupancy of electrons in the three M and K valleys as a function of the applied electric field in bulk Al_4SiC_4.

0.119% of the total number of electrons simulated. This indicates that electron transport in the material is close to a breakdown due to excessive impact ionization at an electric field of 1400 kV cm^{-1}. This result indicating onset of impact ionization supports our calculated critical electric field of 1831 kV cm^{-1}.

Figures 6 and 7 show electron diffusion and electron mobility as a function of the applied electric field, respectively.

The electron mobility and the electron diffusion decay exponentially as the electric field increases. The electron mobility and electron diffusion at a low electric field are 82.9 cm^2 V^{-1} s^{-1} and 2.1 cm^2 s^{-1}, respectively, which are at their respective maxima, while at a high electric field of 1400 kV cm^{-1}, the values are 9.63 cm^2 V^{-1} s^{-1} and 0.25 cm^2 s^{-1}, respectively.

Figure 8 shows a stacked plot to illustrate the population of electrons occupying each valley (M and K valleys) obtained from the MC simulations. The M valley becomes populated evenly at the start of the simulation as expected until the electrons have enough energy to make a transition into the K valley. The K valley does not start to become populated until approximately 450 kV cm^{-1} but remains <20% populated at the largest electric field, which justifies our approximation of an isotropic K valley.

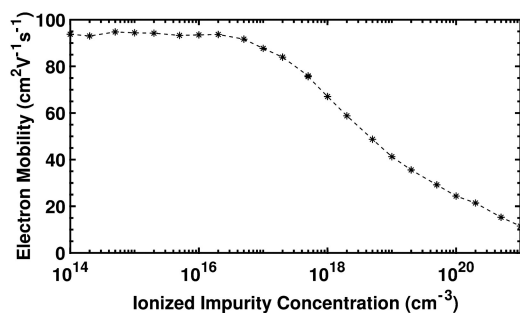Finaly, we examine the relationship between electron mobility and ionized impurity concentration in Figure 9. The

Figure 9. Electron mobility as a function of ionized impurity concentration in bulk Al_4SiC_4.

electron mobility of Al_4SiC_4 has a typical dependence on the ionized impurity concentration when the mobility remains approximately constant until an ionized impurity concentration of 2×10^{16} cm^{-3} is reached. When the ionized impurity concentration increases further, the electron mobility starts to decline to ~10 cm^2 V^{-1} s^{-1} as seen in many semiconductor materials.[20]

5. CONCLUSIONS

The MC simulations of the electron transport in Al_4SiC_4 that has a hexagonal crystal structure have been adapted to include a rotational transformation in the lowest conduction band, the M valley, to account for the strong anisotropy of the electron effective mass. The strong anisotropy of the electron effective mass in the M valley has a profound impact on the electron drift velocity and mobility. The electron effective masses extracted from DFT calculations have shown that there is a large effective mass in both the longitudinal and transverse directions for the K valley of 1.0569 and 0.9360 m_e, respectively, compared with those for the M valley of 0.5678 and 0.6952 m_e, respectively.

The MC simulations allow us to predict the material transport properties of Al_4SiC_4. We have predicted the dependence of the electron drift velocity, electron mobility, average kinetic energy of electrons, and electron population against the applied electric field, all of which can serve as crucial indicators in assessing the electronic and optoelectronic performance of devices. We have shown that the electron drift velocity increases with an increase in the electric field reaching

1.35×10^7 cm s^{-1} to approximately 1400 kV cm^{-1}. The electron kinetic energy has a linear increase as expected and reaches 1.24 eV at 1400 kV cm^{-1}. The threshold energy barrier when electrons start to be transferred from the M valley to the K valley occurs at an electric field of approximately 450 kV cm^{-1}. We predict that the number of electrons with a higher energy that is greater than the band gap of the material will start to increase rapidly as the electric field draws closer to the critical field of 1831 kV cm^{-1}, causing a breakdown to occur.

The electron mobility decreases with an increase in the electric field from approximately 82.9 to 9.6 cm^2 V^{-1} s^{-1}, and the diffusion decreases from approximately 2.14 to 0.25 cm^2 s^{-1}, both over a range of very low electric fields to 1400 kV cm^{-1}. Finally, we have shown that the electron mobility is dependent on the ionized impurity concentration, declining from its maximum value of 82.9 cm^2 V^{-1} s^{-1} at low doping concentrations of $\leq 2 \times 10^{16}$ cm^{-3} to ~10 cm^2 V^{-1} s^{-1} at a very high doping concentration of 10^{21} cm^{-3}. These predicted material properties show a limited usage of the Al_4SiC_4 in a channel of potential metal oxide semiconductor field effect transistors (MOSFETs) due to a maximum drift velocity and electron mobility of 1.35×10^7 cm s^{-1} and 83 cm^2 V^{-1} s^{-1}, respectively. Upon comparison of these two material properties of Al_4SiC_4 with properties of know semiconductor materials, the maximum drift velocity of Al_4SiC_4 is only 61.4% of the maximum drift velocity of GaN (2.2×10^7 cm s^{-1}) and the electron mobility of Al_4SiC_4 is 6.7% of the electron mobility of GaN (1250 cm^2 V^{-1} s^{-1}).[29] The maximum drift velocity of Al_4SiC_4 is only 67.5% of that of 6H-SiC (2×10^7 cm s^{-1}), and the electron mobility of Al_4SiC_4 is only 16.6% of that of 6H-SiC (500 cm^2 V^{-1} s^{-1}).[29] Finally, the maximum drift velocity of Al_4SiC_4 is 135% of that of silicon (1×10^7 cm s^{-1}) and the electron mobility of Al_4SiC_4 is only 5.5% of that of silicon (1500 cm^2 V^{-1} s^{-1}).[29]

■ AUTHOR INFORMATION

Corresponding Author
*E-mail: s.forster.661270@swansea.ac.uk.

ORCID ⊙
Simon Forster: 0000-0002-5285-4353
Didier Chaussende: 0000-0002-4180-8749

Notes
The authors declare no competing financial interest.

■ REFERENCES

(1) Liao, T.; Wang, J.; Zhou, Y. Atomistic deformation modes and intrinsic brittleness of Al_4SiC_4: A first-principles investigation. *Phys. Rev. B: Condens. Matter Mater. Phys.* **2006**, *74*, 174112.

(2) Li, Y. F.; Xiao, B.; Sun, L.; Gao, Y. M.; Cheng, Y. H. Phonon optics, thermal expansion tensor, thermodynamic and chemical bonding properties of Al4SiC4 and Al4Si2C5: a first-principles study. *RSC Adv.* **2016**, *6*, 43191−43204.

(3) Hussain, A.; Aryal, S.; Rulis, P.; Choudhry, M. A.; Ching, W. Y. Density functional calculations of the electronic structure and optical properties of the ternary carbides Al4SiC4 and Al4Si2C5. *Phys. Rev. B: Condens. Matter Mater. Phys.* **2008**, *78*, 195102.

(4) Pedesseau, L.; Even, J.; Modreanu, M.; Chaussende, D.; Sarigiannidou, E.; Chaix-Pluchery, O.; Durand, O. Al4SiC4 wurtzite

crystal: Structural, optoelectronic, elastic, and piezoelectric properties. *APL Mater.* **2015**, *3*, 121101.

(5) Zevgitis, D.; Chaix-Pluchery, O.; Doisneau, B.; Modreanu, M.; La Manna, J.; Sarigiannidou, E.; Chaussende, D. Synthesis and Characterization of Al4SiC4: A "New" Wide Band Gap Semiconductor. *Mater. Sci. Forum* **2015**, *821-823*, 974−977.

(6) Pedesseau, L.; Chaix-Pluchery, O.; Modreanu, M.; Chaussende, D.; Sarigiannidou, E.; Rolland, A.; Even, J.; Durand, O. Al4SiC4 vibrational properties: density functional theory calculations compared to Raman and infrared spectroscopy measurements. *J. Raman Spectrosc.* **2017**, *48*, 891−896.

(7) Inoue, K.; Yamaguchi, A. Synthesis of Al4SiC4. *J. Am. Ceram. Soc.* **2003**, *86*, 1028−1030.

(8) Inoue, K.; Yamaguchi, A.; Hashimoto, S. Fabrication and oxidation resistance of A(14)SiC(4) body. *Nippon Seramikkusu Kyokai Gakujutsu Ronbunshi* **2002**, *110*, 1010−1015.

(9) Ching, W.; Rulis, P. *Electronic Structure Methods for Complex Materials: The Orthogonalized Linear Combination of Atomic Orbitals*; Oxford University Press: Oxford, U.K., 2012.

(10) Deng, C.; Kuang, J.; Zhu, H.; Bai, C. Effects of Fe2O3 on synthesis of Al4SiC4/Al4O4C composite refractory from natural raw materials. *Guisuanyan Xuebao* **2010**, *8*, 049.

(11) Yamaguchi, A.; Zhang, S. Synthesis and some properties of Al4SiC4. *Nippon Seramikkusu Kyokai Gakujutsu Ronbunshi* **1995**, *103*, 20−24.

(12) Zhao, J.; Lin, W.; Yamaguchi, A.; Ommyoji, J.; Sun, J. Synthesis of Al4SiC4 from alumina, silica and graphite. *J. Ceram. Soc. Jpn.* **2007**, *115*, 761−766.

(13) Yamamoto, O.; Ohtani, M.; Sasamoto, T. Preparation and oxidation of Al4SiC4. *J. Mater. Res.* **2002**, *17*, 774−778.

(14) Schoennahl, J.; Willer, B.; Daire, M. The mixed carbide Al4SiC4 - Preparation and Structural Data. *J. Solid State Chem.* **1984**, *52*, 163−173.

(15) Le-Tran, H.-L.; Sarigiannidou, E.; Gélard, I.; Chaussende, D. Vaporization and condensation in the Al4C3-SiC system. *J. Eur. Ceram. Soc.* **2017**, *37*, 4475−4482.

(16) Sun, L.; Gao, Y.; Li, Y.; Yoshida, K.; Yano, T.; Yi, D. Structural, bonding, anisotropic mechanical and thermal properties of Al4SiC4 and Al4Si2C5 by first- principles investigations. *Journal of Asian Ceramic Societies* **2016**, *4*, 289−298.

(17) Li, Y.; Xiao, B.; Sun, L.; Gao, Y.; Cheng, Y. A theoretical study of dielectric tensor, Born effective charges, LO-TO splitting and infrared response of Al4SiC4 and Al4Si2C5. *J. Alloys Compd.* **2017**, *692*, 713−719.

(18) Al-Nasrawy, D. K. M.; Ahmed Al-Sarraj, Z. S.; Issa, T. T.; Jassim, S. G. H. Observations on the Electrical Properties of Al-Sic Composite. *Journal of Al-Nahrain University-Science* **2012**, *15*, 120−128.

(19) Aldegunde, M.; Kalna, K. Energy conserving, self- force free Monte Carlo simulations of semiconductor devices on unstructured meshes. *Comput. Phys. Commun.* **2015**, *189*, 31−36.

(20) Islam, A.; Kalna, K. Monte Carlo simulations of mobility in doped GaAs using self- consistent fermidirac statistics. *Semicond. Sci. Technol.* **2011**, *26*, 055007.

(21) Barczak, V. Optical and X-Ray Powder Diffraction Data for Al4SiC4. *J. Am. Ceram. Soc.* **1961**, *44*, 299.

(22) Solozhenko, V.; Kurakevych, O. Equation of state of aluminum silicon carbide alpha-Al4SiC4. *Solid State Commun.* **2005**, *135*, 87−89.

(23) Forster, S.; Canas, J.; Lloret, F.; Gutierrez, M.; Araujo, D.; Kalna, K.; Chaussende, D. Experimental Extraction of the Bandgap for Al4SiC4. *Proceedings of UK Semiconductors*, Sheffield, UK, July 4−5, 2018.

(24) Morales-Garcia, A.; Valero, R.; Illas, F. An Empirical, yet Practical Way To Predict the Band Gap in Solids by Using Density Functional Band Structure Calculations. *J. Phys. Chem. C* **2017**, *121*, 18862−18866.

(25) Elmessary, M. A.; Nagy, D.; Aldegunde, M.; Seoane, N.; Indalecio, G.; Lindberg, J.; Dettmer, W.; Perić, D.; García-Loureiro, A. J.; Kalna, K. Scaling/LER study of Si GAA nanowire FET using 3D finite element Monte Carlo simulations. *Solid-State Electron.* **2017**, *128*, 17−24.

(26) Iwata, H.; Itoh, K. Donor and acceptor concentration dependence of the electron Hall mobility and the Hall scattering factor in n-type 4H-and 6H-SiC. *J. Appl. Phys.* **2001**, *89*, 6228−6234.

(27) Hudgins, J. L.; Simin, G. S.; Santi, E.; Khan, M. A. An Assessment of Wide Bandgap Semiconductors for Power Devices. *IEEE Transactions on Power Electronics* **2003**, *18*, 907−915.

(28) Herring, C.; Vogt, E. Transport and deformation - potential theory for many- valley semiconductors with anisotropic scattering. *Phys. Rev.* **1956**, *101*, 944−961.

(29) Ozpineci, B.; Tolbert, L. M. Comparison of Wide-Bandgap Semiconductors for Power Electronics Applications. Technical Report ORNL/TM-2003/257; Oak Ridge National Laboratory: Oak Ridge, TN, 2004.